

Comparison of numerical hindcasted severe waves with Doppler radar measurements in the North Sea

Sonia Ponce de León¹ · João H. Bettencourt¹ · Frederic Dias¹

Received: 8 January 2016 / Accepted: 1 November 2016 / Published online: 18 November 2016
© Springer-Verlag Berlin Heidelberg 2016

Abstract Severe sea states in the North Sea present a challenge to wave forecasting systems and a threat to offshore installations such as oil and gas platforms and offshore wind farms. Here, we study the ability of a third-generation spectral wave model to reproduce winter sea states in the North Sea. Measured and modeled time series of integral wave parameters and directional wave spectra are compared for a 12-day period in the winter of 2013–2014 when successive severe storms moved across the North Atlantic and the North Sea. Records were obtained from a Doppler radar and wave buoys. The hindcast was performed with the WAVEWATCH III model (Tolman 2014) with high spectral resolution both in frequency and direction. A good general agreement was obtained for integrated parameters, but discrepancies were found to occur in spectral shapes.

Keywords Wind waves · North Sea · Microwave Doppler wave radar · MIROS radar · WAVEWATCH III · Wave spectra

1 Introduction

The North Sea is a major world economic region where a large range of human activities take place. These activities include

This article is part of the Topical Collection on *the 14th International Workshop on Wave Hindcasting and Forecasting in Key West, Florida, USA, November 8–13, 2015*

Responsible Editor: Jose-Henrique Alves

✉ Sonia Ponce de León
sonia.poncedeleonalvarez@ucd.ie

¹ School of Mathematics and Statistics, UCD Earth Institute, University College Dublin, Dublin, Ireland

fisheries, oil and gas extraction and transport, shipping, and offshore renewable energy production. The highly developed industrial landscape of the North Sea implies significant capital investment and human presence and increased environmental risks should an accident occur. Mobile and fixed equipment in this area are subject to harsh environmental conditions such as those of storm Britta in 2006 when several ship and offshore platforms experienced operational difficulties and damages due to high waves (Kettle 2015). The capability of forecasting accurately the occurrence of these severe conditions and also their magnitude is of great importance for avoiding human and economic losses.

The sea state in the North Sea varies from gentle to severe (Boukhanovsky et al. 2007; Reistad et al. 2011; Ponce de León and Guedes Soares 2012). Extreme sea states generated under hurricane force storms appear to be frequent (Behrens and Gunther 2009), and several rogue wave events have been recorded (Magnusson and Donelan 2013; Haver and Andersen 2000; Haver 2000; Fedele et al. 2016).

The knowledge about extreme waves and their forecast are very important challenges to the scientific community, for reasons related with the scientific understanding of their causes and how they propagate and disappear as well as for the safety of navigation and prevention of damage to offshore structures and ships. While the severity of a sea is usually measured from integral parameters such as the significant wave height (H_s), the shape of the frequency-direction spectrum plays an important role in the probability of occurrence of extreme waves.

The present study analyzes sea states in the North Sea during a period of the winter of 2013–2014 when several storms occurred. High-resolution wave hindcasts were conducted with the WW3 model (version 4.18), and integral parameters, frequency, and directional spectra were compared to measurements obtained by a pulse-Doppler wave radar.

Attention was focused on the comparison of the shapes of the spectra.

This paper is structured as follows: Sect. 2 describes the North Sea and Sect. 3 treats the details of the configuration of the WW3 model used for the hindcast. In Sect. 4, details are given about the wave radar and the measurements used in the comparison. Section 5 presents the validation of the hindcasts. Results of the comparison of frequency and directional wave spectra between the radar and the model are given in Sect. 6, and the conclusions are given in Sect. 7.

2 Region and period of study

The North Sea, due to its complex geometry and bathymetry (Fig. 1), reveals complicated synoptic conditions for wind waves. It is connected to the Baltic Sea and, by the English Channel and the Norwegian Sea, to the North Atlantic. Due to its geometry, severe winds from different directions have a great impact in its coastal regions (De Winter et al. 2013). The north part of the North Sea is characterized by deep waters, and the central and south parts are mainly intermediate waters ranging from 50 to 75 m, where most of the offshore platforms are located.

The period of study is a 12-day window of the winter of 2013–2014, characterized by an extraordinary duration of storms and a clustering of deep depressions (Met Office 2014). During that winter, the combination of a very intense polar vortex and an unusually strong North Atlantic jet stream caused a succession of strong low-pressure systems to cross the Atlantic (Davies 2015), which reached and impacted the European coastal zones. According to Masselink et al. (2016),

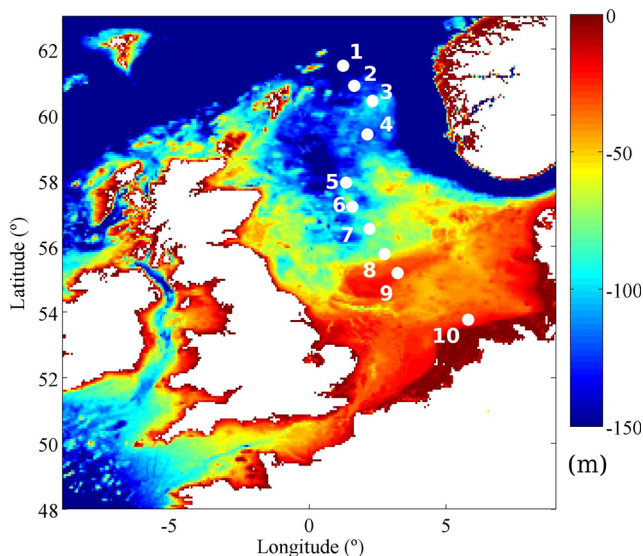


Fig. 1 The North Sea bathymetry, the WW3 output, and wave buoy locations. 1–Gullafks, 2–North Alwyn, 3–Troll, 4–Heimdal, 5–Sleipner, 6–Mungo, 7–Ulla, 8–Ekofisk, 9–Valhall, 10–Fino1

the 2013–2014 winter was the most energetic along most of the Atlantic coast of Europe since at least 1948. A notorious storm of this period was the Hercules storm of January 2014, whose effects on the Iberian Peninsula were discussed in Ponce de León and Guedes Soares (2015).

During the 12-day period that is analyzed, an intense depression passed to the north of the UK on 24 December 2013, with a mean sea level pressure of 936 mb (Met Office 2014). Pressures below 950 mb were reported at UK land stations. These values are the lowest that have been observed at UK land stations for many years. The European Centre for Medium-Range Weather Forecasts (ECMWF) wind field (Fig. 2) shows stormy conditions over the North Sea on 25 December 2013 at 05:00 UTC.

Because the period of this study is characterized by successive severe storms generated from low-pressure systems that crossed the North Atlantic, the winds in the North Sea have a predominant direction from SW and south in accordance with the cyclonic circulation. From 05 to 06 December 2013 at 18:00 UTC, very strong winds blew from the NW along the main axis of the North Sea, where the fetch is larger, generating significant wave heights of about 9 m at Sleipner (location 5). From 20 to 29 December 2013, the wind blew mainly from the SW towards Norway, where the fetch is shorter. However, in the north part of the North Sea, the wind speed and H_s were noticeably high on 25 December 2013 (Fig. 2), reaching approximately 25 m/s and values above 8 m, respectively.

3 The WAVEWATCH III model setup

WW3 is a third-generation spectral wave model developed at NOAA/NCEP based on the WAM model (Komen et al. 1994). Ocean wave models such as WW3 are based on the spectral energy balance (Eq. (1)),

$$\frac{\partial F(f, \theta)}{\partial t} + \nabla_x \cdot \vec{c}_x F(f, \theta) + \nabla_{f, \theta} \cdot \vec{c}_{f, \theta} F(f, \theta) = S(f, \theta) \quad (1)$$

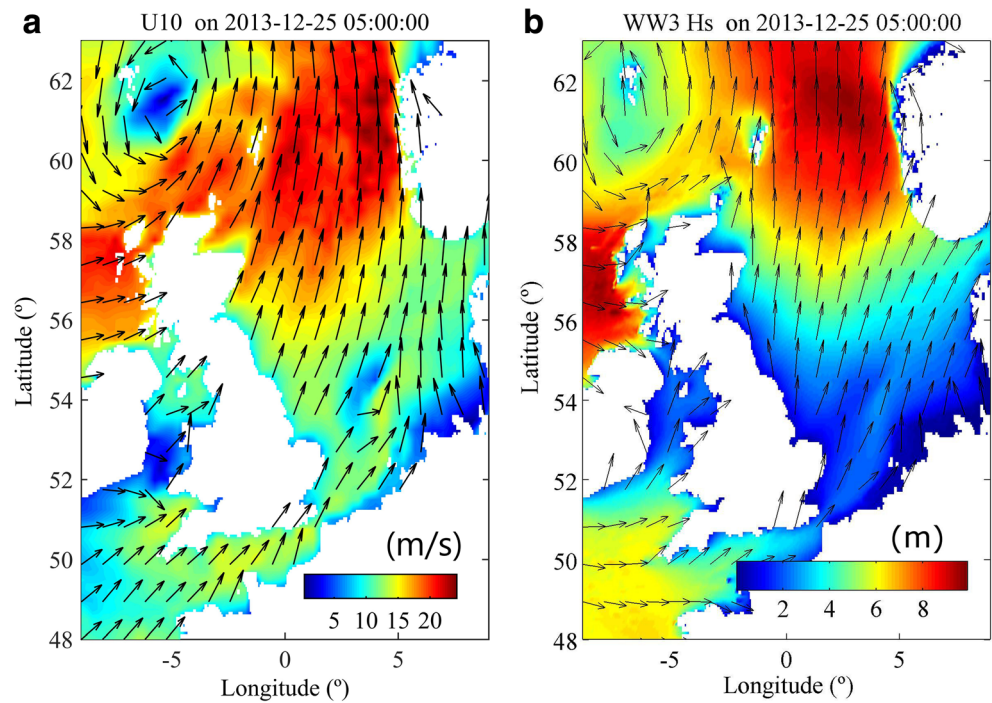
where f and θ are the spectral frequency and direction; F is the energy spectrum; \vec{c}_x and $\vec{c}_{f, \theta}$ are the characteristic velocities in the physical and spectral spaces, respectively; and ∇_x and $\nabla_{f, \theta}$ are the gradient differential operators. S is the total source function in which all the physical processes considered in WW3 are represented:

$$S = S_{in} + S_{nl} + S_{ds} \quad (2)$$

There are three main contributions to S , wind input (S_{in}), wave-wave nonlinear interactions (S_{nl}), and wave energy dissipation due to wave breaking and shallow water processes (S_{ds}).

The hindcast was conducted using nesting of computational spatial grids. The coarse grid domain was set to 80°N–

Fig. 2 ECMWF wind speed (m/s) (a) and the WW3 H_s (m) (b) map from the high-resolution nested grid on 25 December 2013 at 05:00 UTC



18°N, 90°W–30°E at spatial resolution of 0.25°, covering almost the entire North Atlantic basin. The first nested grid (intermediate grid in Table 1) was defined by the following limits: 66°N–47°N, 35°W–15°E at the spatial resolution of 0.125°. The high-resolution nested grid was defined over the North Sea region with a resolution of 0.0625° and the following limits: 63°N–48°N, 9°W–

9°E (Fig. 2). The wave spectrum was computed in 36 directional bands and 30 frequencies from the minimum frequency of 0.0350 up to 0.5552 Hz. Other numerical parameters are given in Table 1.

The hindcast was performed for 2 months and 15 days for the winter of 2013–2014. The wave model was driven by hourly wind fields from the ECMWF operational forecast

Table 1 Configuration of computational grids and physics for WW3

Parameters	Coarse grid North Atlantic	Intermediate nested grid	High-resolution nested grid
Geographical limits	80°N–18°N, 90°W–30°E	66.0°N–47°N, 35°W–15°E	63°N–48°N, 9°W–9°E
Spatial resolution	0.25°	0.125°	0.0625°
Number of points	(481,249) 119,769	(401,153) 61,353	(289,241) 69,649
Type of spectral model	Deep water	Deep water	Shallow water
Propagation	Spherical	Spherical	Spherical
Wind input (S_{in})	Janssen (1989, 1991)	Janssen (1989, 1991)	Janssen (1989, 1991)
White capping dissipation	Komen et al. (1984)	Komen et al. (1984)	Komen et al. (1984)
Nonlinear interactions (S_{nl})	Four wave-wave nonlinear interactions	Four wave-wave nonlinear interactions	Triad interactions (Eldeberky 1996)
Bottom friction dissipation (S_{bofr})	JONSWAP	JONSWAP	JONSWAP
Wind input time step (h)	1	1	1
Wave model output time step (h)	1	1	1
Integration time step (s)	120	60	30
Wind data	ECMWF operational forecast	ECMWF operational forecast	ECMWF operational forecast
Bathymetry data	GEODAS NOAA's	GEODAS NOAA's	GEODAS NOAA's
SIN3 maximum value of wind-wave coupling	BETAMAX = 1.40	BETAMAX = 1.40	BETAMAX = 1.40

retrieved from the MARS archive with a horizontal resolution of 16 km.

The bathymetric data was extracted from the ETOPO1 1 arc-minute global relief model distributed by the NOAA National Center for Environmental Information (NCEI) and was linearly interpolated to the three model grids.

A shallow water configuration was used in the nested grid over the North Sea (Table 1). Regarding the physical and numerical aspects, the following processes and parameters were activated for the North Sea fine grid: wind input and dissipation of energy (ST3) from WAM cycle 4 (Komen et al. 1994), JONSWAP bottom friction formulation, the lumped triad-interaction method based on the stochastic model of Eldeberky (1996), the discrete interaction approximation (DIA) (Hasselmann et al. 1985), depth-induced breaking of Battjes and Janssen (1978) with a breaking threshold of 0.73 and refraction; for the propagation of the spectral wave energy along the geographical domain, a third-order propagation scheme was chosen using Tolman's (2002) averaging technique. Reflection, ice, and currents were not considered in this hindcast.

4 Sources of measured data

4.1 Microwave pulse-Doppler radar

The MIROS SM-050 radar is a C-band (5.17 GHz) pulse-Doppler radar that works by sending a radar signal at a frequency that responds to capillary waves. The returned signal has a Doppler shift that depends on the speed of the water particles. After extracting an average current speed, the spectrum of the velocity fluctuations is transformed into a wave energy spectrum using linear wave theory. The MIROS radar scans the ocean surface in a semi-circle, with six antennas covering 30° sectors each. The installation in Sleipner A observes the sector 045–225, clockwise from the north, from a height of 76 m above mean sea level. The observation distance is ~450 m, and the observational footprint is 75 m deep in the horizontal. Each sector is sampled for 2.5 min. In this particular dataset, no averaging is carried out.

Some studies comparing integral wave parameters such as those of Dobson and Dunlap (1999) and Ribeiro et al. (2013) found an excellent agreement between MIROS and buoy data. Additionally, the data from several MIROS radar installations has been used to perform validation studies of numerical models, such as the validation of the NORA 10 hindcast model by the Meteorological Office of Norway (Reistad et al. 2015).

The radar also provided time series of spectrum integral parameters with a measurement frequency of 10 min (location 5; Fig. 1) during 12 days (20 to 31 December 2013).

4.2 Wave buoys (Joint Technical Commission for Oceanography and Marine Meteorology project)

The study used wave buoy data from 10 different locations in the North Sea (Fig. 1), distributed by the Joint Technical Commission for Oceanography and Marine Meteorology (JCOMM) project (Bidlot 2012). These moorings consist of directional and nondirectional wave buoys transmitting hourly data on the standard suite of meteorological parameters. The mean wave direction was recorded in only one of the wave buoys (location 10). The buoy time series were checked for invalid data which were subsequently removed. The wave buoy data was used as reference data to validate both model and radar.

5 Validation of the hindcast

The statistical parameters employed in the validation of the hindcast against the wave buoys were the correlation coefficient, bias, and scatter index. The bias is defined as the mean of the residual, which is the difference between the buoy data and model data, and the scatter index (SI) is defined as the standard deviation of the model data from the best fit line, divided by the mean of the observations. The model H_s of the fine grid was validated with 10 wave buoys.

The statistical parameters (Table 2) reveal a good agreement of the model results with a linear correlation for the H_s . The correlation coefficients (CCs) were in the range of 0.850 (location 10) to 0.961 (location 2), and the SIs were in the range of 0.111 (location 2) to 0.292 (location 10). The biases turned out to be negative (records were taken as reference) in five locations (3, 4, 6, 7, 9), indicating that the WW3 model overestimates the recorded values of H_s at those locations.

Table 2 Statistical parameters for the H_s at the following locations: 1–Gullafks, 2–North Alwyn, 3–Troll, 4–Heimdal, 5–Sleipner, 6–Mungo, 7–Ullabnor, 8–Ekofisk, 9–Valhall, and 10–Fino1 (see Fig. 1)

Location	Bias (m)	Scatter index	CC
1	0.289	0.137	0.938
2	0.056	0.111	0.961
3	−0.096	0.179	0.892
4	−0.296	0.146	0.910
5	0.277	0.137	0.949
6	−0.212	0.129	0.922
7	−0.167	0.130	0.948
8	0.094	0.136	0.951
9	−0.135	0.131	0.960
10	0.064	0.292	0.850

CC correlation coefficient

The lowest CC (0.850) and the highest SI (0.292) were obtained at location 10 (FINO1) placed in intermediate waters at 30 m of depth, which could be a possible reason for the low correlation (Table 2). Similarly, low values of correlation have been reported in Gallagher et al. (2016) and Ponce de León et al. (2016) for the Irish Sea and the Mediterranean Sea, respectively.

Regarding the underperformance of the wave model at location 10, it is possible that despite of the grid high resolution in space, time, and in the spectral domain, additional effects may come into play when moving towards the coast. Moreover, coastal areas are often influenced by strong currents. Our wave model configuration neglects the coupling between waves and currents, which could be important for the North Sea.

Recent studies have shown that wave model results can be strongly improved by taking into account currents and their effects on wave refraction, enhanced wave breaking, and change in relative wind speeds. Roland and Arduin (2014) have revealed that in the coastal zones of the French Atlantic and Channel coasts, WAVEWATCH III model errors have been strongly reduced due to the introduction of currents, coastal reflection, and bottom sediment types. In addition, bottom friction plays an important role in the coastal zone and may have a significant effect on swell propagation in the North Sea (Van Vledder and Gautier 2015).

Furthermore, location 10 is near the coast (approximately 40 km) in the southern part of the North Sea. This can lead to some difficulties for a wave model to reproduce different wave patterns typical of the North Sea, especially when the wind comes from the land and the fetch is short as in the case of location 10.

The wind speed from the ECMWF atmospheric high-resolution model used in the hindcast was verified with buoy data across the North Sea (Fig. 1). The wind speed recorded by the buoys was corrected to 10 m according to the neutral logarithmic profile described in Bidlot et al. (2002).

Table 3 summarizes the statistics for the wind. The CCs for the wind speed (U_{10}) range from 0.859 (location 9) to 0.967 (location 1), the biases from -1.838 (location 9) to -0.020 (location 3), and the SIs from 0.090 (location 5) to 0.205 (location 9). The CCs for the wind direction φ range from 0.836 (location 1) to 0.958 (location 5), the biases from 0.827 (location 1) to -64.758 (location 7), and the SIs from 0.090 (location 5) to 0.250 (location 7). In general, a good agreement was obtained between the wind speed from the buoys and the high-resolution ECMWF wind.

6 Comparison of model results and radar measurements

In this section, model results are compared to the measurements of the microwave pulse-Doppler radar. In addition to

Table 3 Wind speed at 10 m of height (U_{10}) and wind direction (φ) validation table for the period of 01 December 2013 to 14 February 2014 at 23:00 UTC

Parameters	Bias (m/s; deg)		Scatter index		CC	
	U_{10}	φ	U_{10}	φ	U_{10}	φ
Location	U_{10}	φ	U_{10}	φ	U_{10}	φ
1	1.133	0.827 (-0.113)	0.103	0.186	0.967	0.836
2	0.174	–	0.125	–	0.945	–
3	0.020	-3.630 (-3.945)	0.112	0.165	0.958	0.882
4	0.479	-10.185 (-0.296)	0.106	0.182	0.961	0.893
5	0.213	-2.334 (0.103)	0.090	0.090	0.965	0.958
6	0.025	-2.204 (0.096)	0.173	0.110	0.878	0.922
7	0.098	-64.758 (-0.163)	0.116	0.250	0.933	0.935
8	0.035	–	0.108	–	0.945	–
9	1.838	-10.841 (-0.135)	0.205	0.099	0.859	0.942
10	–	–	–	–	–	–

Records are taken from the JCOMM project wave buoys and compared against time series from the high-resolution atmospheric model ECMWF. In parenthesis, the directional bias is given (Mardia and Jupp 2000)

CC correlation coefficient

the frequency spectrum and the directional spectrum, the radar also provides times series of integral parameters such as H_s and mean wave propagation direction. Wind speed and direction are also provided as time series by the radar, but these are measured by a different sensor.

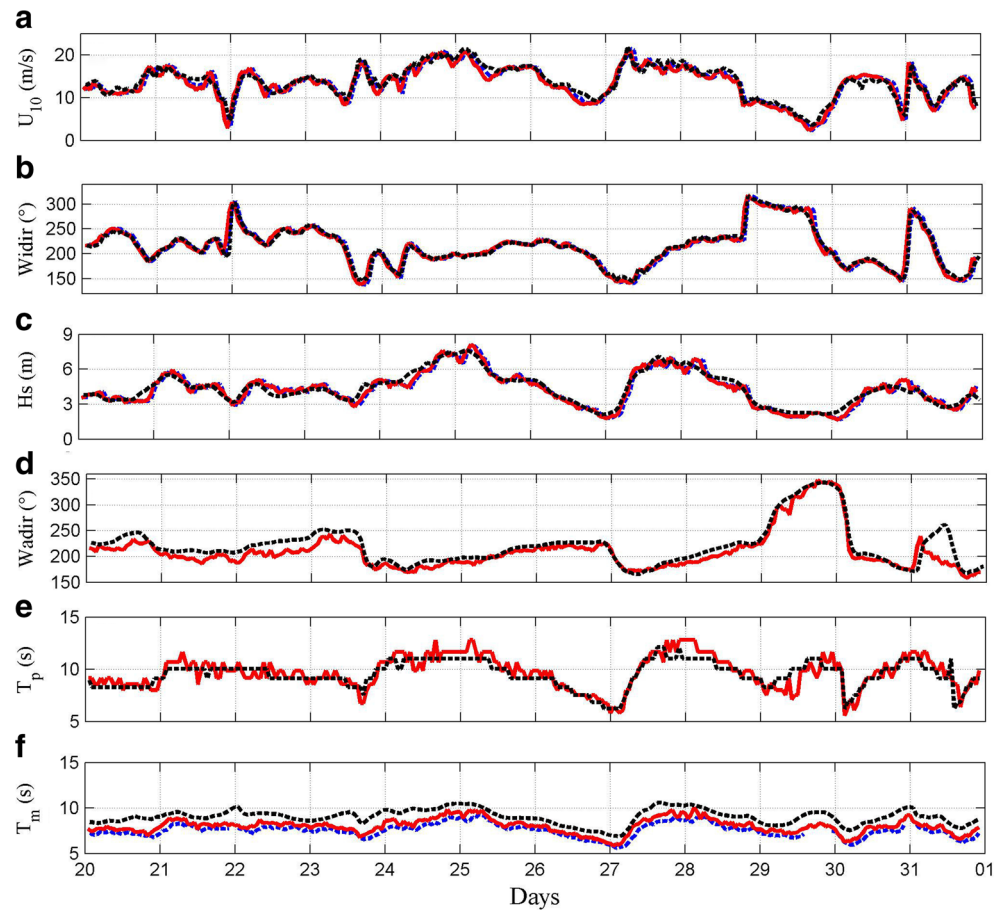
6.1 Wind and integral wave parameters

The evolution in time of the U_{10} (Fig. 3a) presents the following two maxima: the first one of 21.66 m/s (MIROS radar) and 21.25 m/s (ECMWF wind) on 25 December 2013 at 03:00 UTC and the second one of 21.06 m/s (MIROS radar) and 19.59 m/s (ECMWF wind) on 27 December 2013 at 07:00 UTC, corresponding to two different storms. For both storms, the wind was blowing from the southwest (Fig. 3b), while for the lowest wind speeds, the wind came from the northwest.

The time series for H_s clearly shows the duration of the first and second storms (Fig. 3c). The highest H_s recorded by the radar was 8.02 m on 25 December 2013 at 05:00 UTC (Fig. 3c). However, the wave model underestimated the H_s (7.28 m). The second maximum took place on 27 December 2013 at 20:00 UTC, and it is 7.07 m (radar) and 6.67 m (model).

The mean wave propagation direction (Fig. 3d) remained approximately constant from the south-southwest during the first storm, while for the second storm, it rotated steadily from southeast to southwest. Peak periods (T_p ; Fig. 3e) at the two storms were similarly around 12 s. The WW3 mean wave period (Tm01; Fig. 3f) results are overestimated compared to

Fig. 3 Time series comparison of U_{10} (a), wind direction (b), H_s (c), mean wave propagation direction (d), peak period (e), and mean period T_{m01} (f) from the MIROS radar, WW3, and the JCOMM wave buoy at Sleipner for the period of the study. Blue dashed line–buoy, red line–MIROS radar, black dashed line–ECMWF for a, b and WW3 for c–f



the measurements. Other studies observed a similar issue in the WW3 performance regarding the mean period (Amrutha et al. 2016).

A statistical analysis for the 12-day period comparing buoy, radar, and model (Table 4) shows that the radar measurements are closer to the buoy than the model ones. Both the radar and the model overestimate H_s and T_p (negative bias), but the radar shows less scatter and higher correlation with the buoy data. Model results systematically overestimate radar measurements, with the bias in the mean wave propagation direction reaching 10° .

6.2 Frequency wave spectra

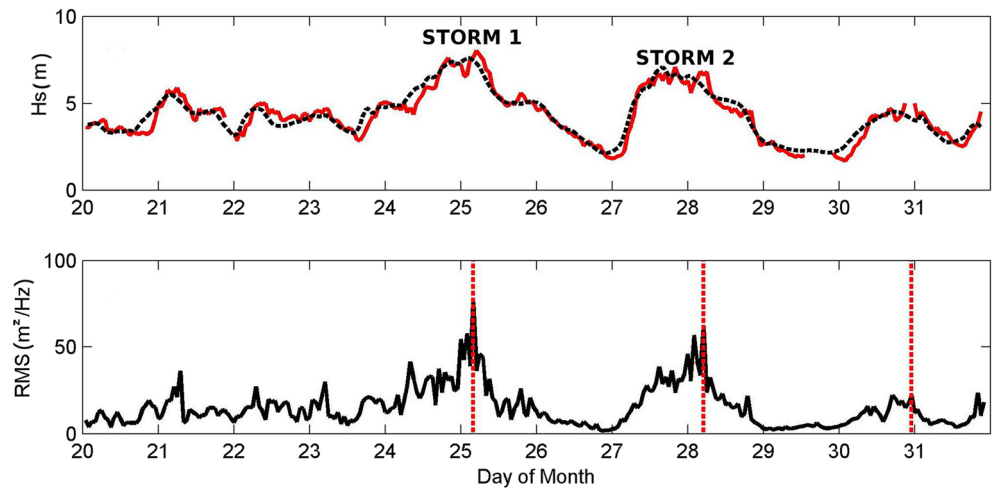
Frequency spectra from model and radar were compared on the basis of the root-mean-square (RMS) difference of the spectral levels at discrete frequencies. The RMS error is computed by interpolating radar spectra to the WW3 frequency grid in the common frequency range. The RMS difference between radar and model frequency spectra was calculated by averaging the squared difference of spectral energy level at each frequency across the common frequency range. It is shown in Fig. 4, where we show again the time series of H_s in order to better visualize in which sea states the highest RMS

Table 4 Statistics for H_s , peak wave period (T_p), and mean wave direction (θ) at Sleipner for the period of 20 to 31 December 2013 at 23:00 UTC

Statistical coefficients	Buoy and MIROS radar			Buoy and WW3			MIROS radar and WW3		
	H_s	T_p	θ	H_s	T_p	θ	H_s	T_p	θ
Bias (m/s; deg)	-0.001	-0.465	-	-0.072	-1.309	-	-0.062	-0.181	-10.352 (-11.391)
Scatter index	0.068	0.024	-	0.101	0.047	-	0.089	0.080	0.059
CC	0.977	0.975	-	0.950	0.915	-	0.964	0.922	0.951

In parenthesis, the directional bias is given (Mardia and Jupp 2000)

Fig. 4 Time series of H_s (m) at location 5 (top) from the MIROS radar and from the WW3 model and root-mean-square (RMS) error (bottom) of WW3 frequency spectra for the period of 20 to 31 December 2013. RMS error computed by interpolating radar spectra to WW3 frequency grid (in the common frequency range). Dashed vertical lines at 25 December 2013 04:00 UTC, 28 December 2013 05:00 UTC and 30 December 2013 23:00 UTC. Red line–radar; black dashed line–model



differences occurred. The two highest differences, which are highlighted by the two left vertical lines in Fig. 4, were obtained during two major storms. The third vertical line (on the right) corresponds to milder conditions, but this case is also of interest. Thus, the attention was focused on those three dates, where an analysis of the one-dimensional spectra and of the respective source functions was performed.

The discrepancies between radar and model frequency wave spectra during the two major storms can be attributed to a slight shift of the spectral peaks in the spectrum of 25 December 2013 at 04:00 UTC (Fig. 5) and in the spectrum of 28 December 2013 at 05:00 UTC (Fig. 6). During the milder event of 30 December 2013, the reason for the discrepancy is different; it is a difference in the level of spectral energy at the peak frequency (Fig. 7).

In order to better understand what might have happened, we analyzed the source functions. In the case of the major storms of 25 and 28 December 2013, the dominant local processes in the spectral energy balance are wind input and wave-wave nonlinear interactions (Fig. 8a, b), which inject energy in the low-frequency range at and below the peak frequency.

In the case of the largest underestimation of the spectral peak by the wave model (on 30 December 2013 at 23:00 UTC), the dominant local process is provided by wave-wave nonlinear interactions (Fig. 8c). The nonlinear interactions (S_{nl}) play a key role in adjusting the total source balance as was demonstrated in Tamura et al. (2010). In addition, there are some differences in the variance density spectra at the high-frequency tails of the spectra, especially on 28 and 30 December 2013 (Figs. 6 and 7), where secondary peaks are

Fig. 5 Frequency spectra at Sleipner on 25 December 2013 at 04:00 UTC. **a** Radar and WW3 spectra. **b** Difference between radar and WW3 spectra

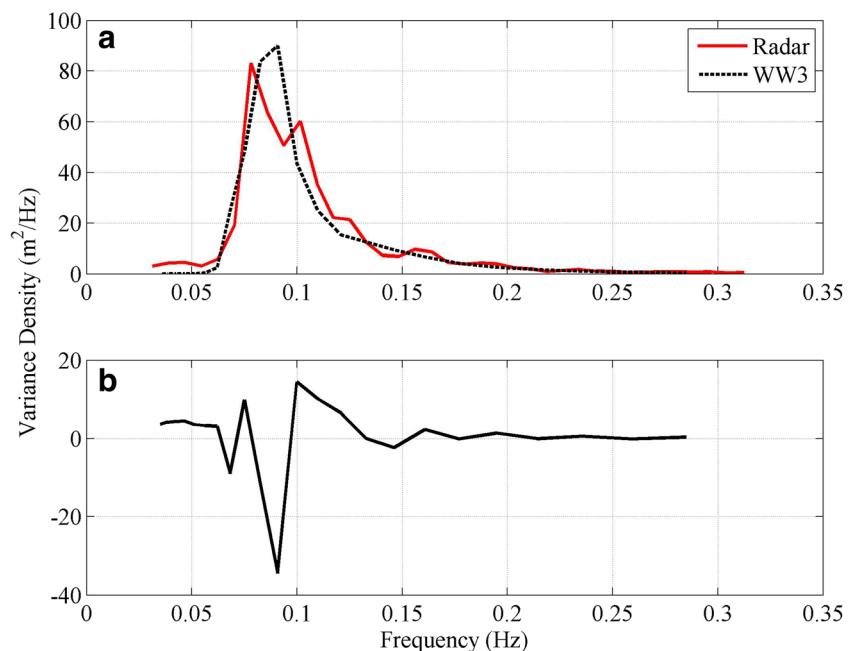
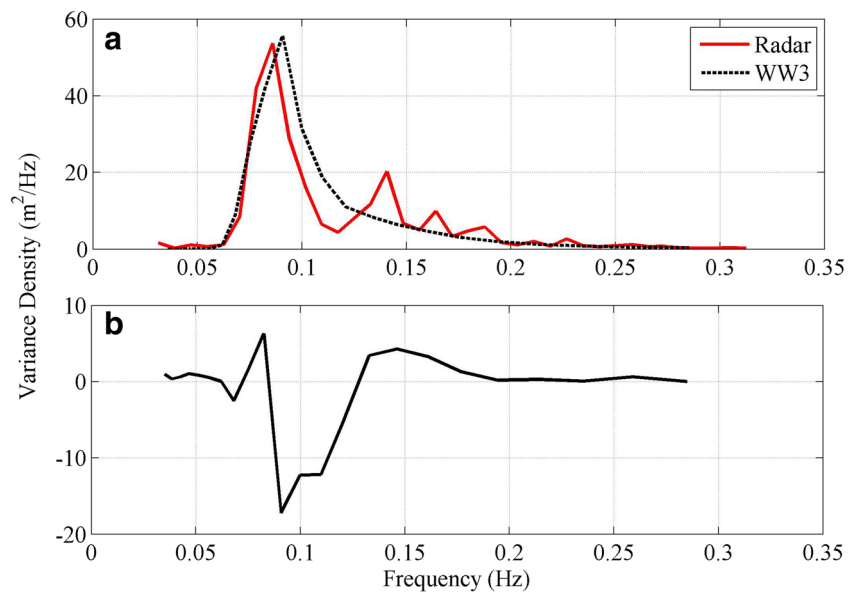


Fig. 6 Frequency spectra at Sleipner on 28 December 2013 at 05:00 UTC. **a** Radar and WW3 spectra. **b** Difference between radar and WW3 spectra



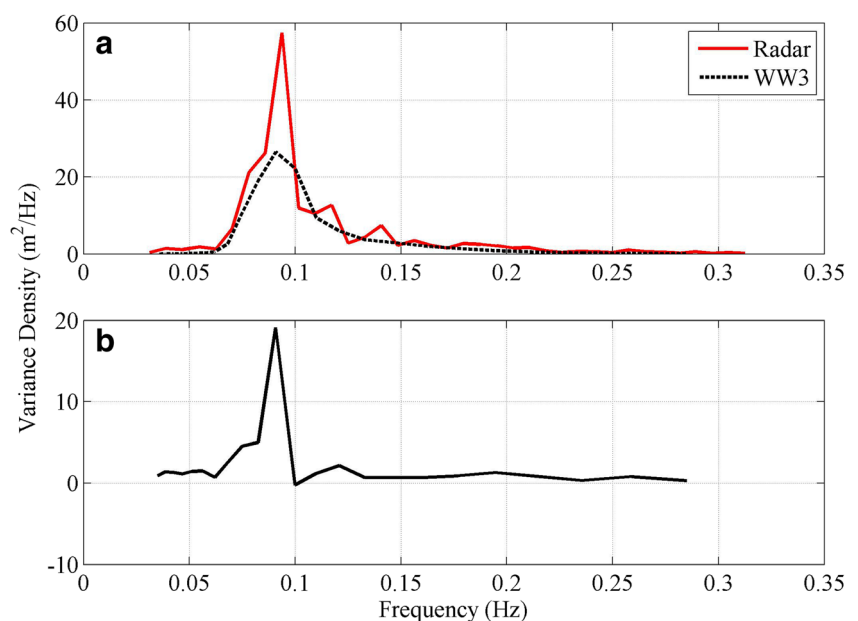
clearly visible in the radar spectra while they are absent in the WW3 spectra.

Since location 5 (Sleipner) is at a deep water location, the bottom friction dissipation (S_{bot}) does not play any role. In the case of the storms on 25 and 28 December 2013, the nonlinear interactions played a secondary role in the spectral balance; on the contrary, on 30 December 2013 when the wind speed was a breeze of about 10 m/s, it can be seen that S_{nl} prevailed and reacted quickly to changes in the source balance.

The differences between modeled and measured wave spectra (Figs. 6 and 7) could be explained by the fact that the radar is showing complex wave systems of the North Sea that the wave model cannot reproduce. A possible explanation could be the fact that the temporal resolution of the

wind fields used in our study is 1 h, implying that the intrinsic variability of the real wind in the North Sea is not captured by the wind field at this time scale (1 h). Similar studies in the 90s (Cavaleri and Burgers 1992; Komen et al. 1994; Ponce de León and Ocampo-Torres 1998) showed that wind gustiness is important in wave generation and may induce stronger surface stress and consequently an enhancement in the wave generation process. In particular, Ponce de León and Ocampo-Torres (1998) studied the effect of the wind variability using realistic wind measurements with time scales of minutes showing that a high variability of the wind induces more complex directional wave spectra with secondary peaks. In addition, their study showed how the wave energy increases with wind variability.

Fig. 7 Frequency spectra at Sleipner on 30 December 2013 at 23:00 UTC. **a** Radar and WW3 spectra. **b** Difference between radar and WW3 spectra



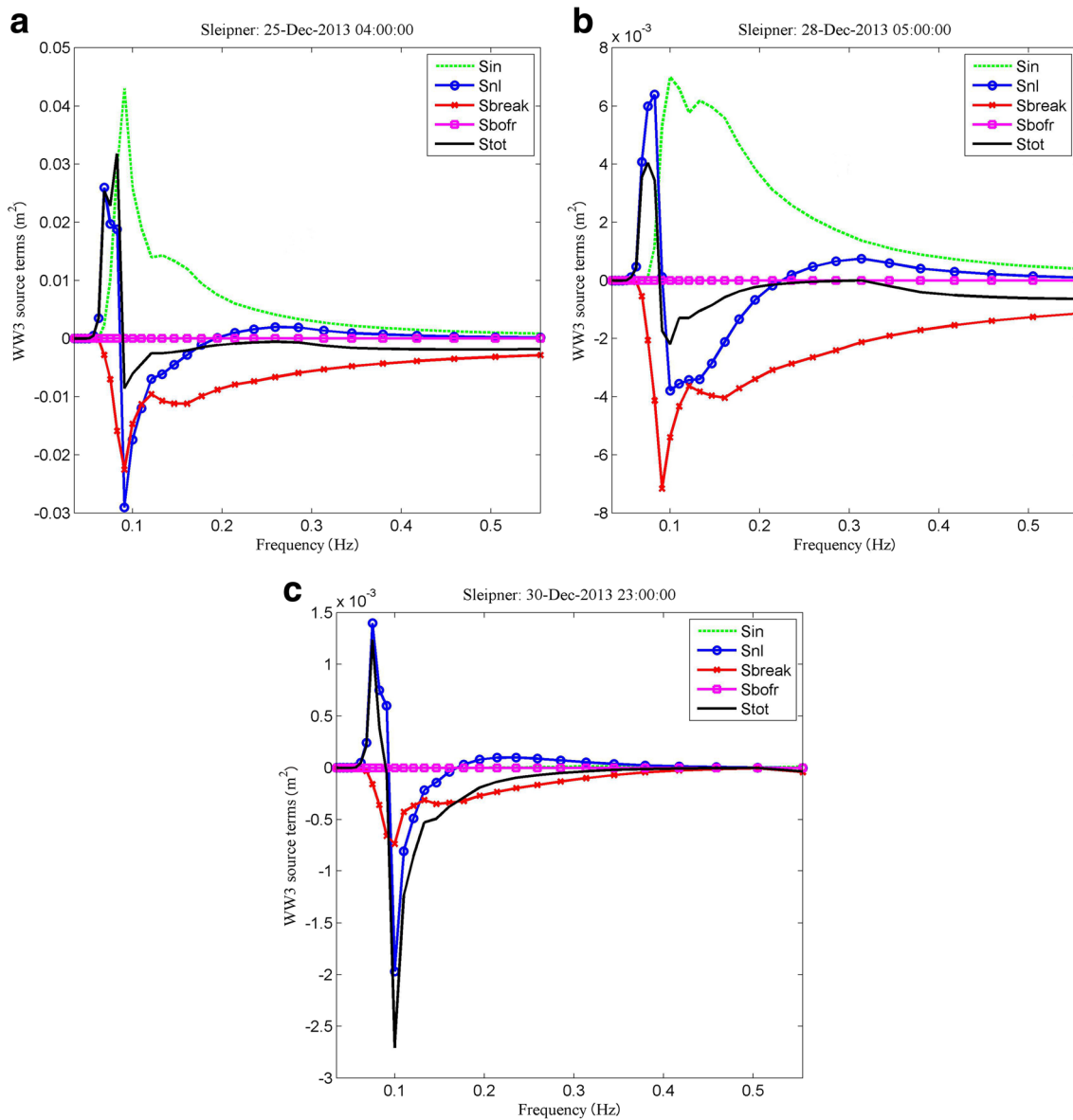


Fig. 8 Source functions (WW3) for **a** 25 December 2013 at 04:00 UTC, **b** 28 December 2013 at 05:00 UTC, and **c** 30 December 2013 at 23:00 UTC. *Sin* wind input, *Snl* wave-wave nonlinear interactions, *Sbreak*

breaking dissipation, *Sbot* bottom friction dissipation, and *Stot* total source function magnitude

6.3 Directional spreading

Directional spreading is one of the parameters that, together with the steepness and the frequency bandwidth, characterizes the shape of a directional wave spectrum. The directional spreading from the wave model was compared to the one recorded by the MIROS radar during the period of study. Prominent differences were found. The highest differences between the hindcast and radar spectra were found during the first storm, which occurred approximately between 24 and 26 December 2013.

Radar records of the directional spreading parameter were taken as a reference, and for the first storm, the differences are

higher than for the second storm (Fig. 9), ranging from 10° up to 23.47°, while for the second storm, the differences ranged between 10° and 18.48°. The duration of the storms was almost 2 days. This means that the radar recorded higher values than the model for both storms. These differences can be very important for the prediction of extreme wave conditions.

The implications of these differences in the directional spreading parameter are reflected in the two-dimensional wave spectra, analyzed in the next section. The poor representation of the directional spreading affects the transition from a normal to dangerous sea state in a wave forecast.

Tamura et al. (2010) obtained similar findings for an oceanic location in the Pacific Ocean. However, their results

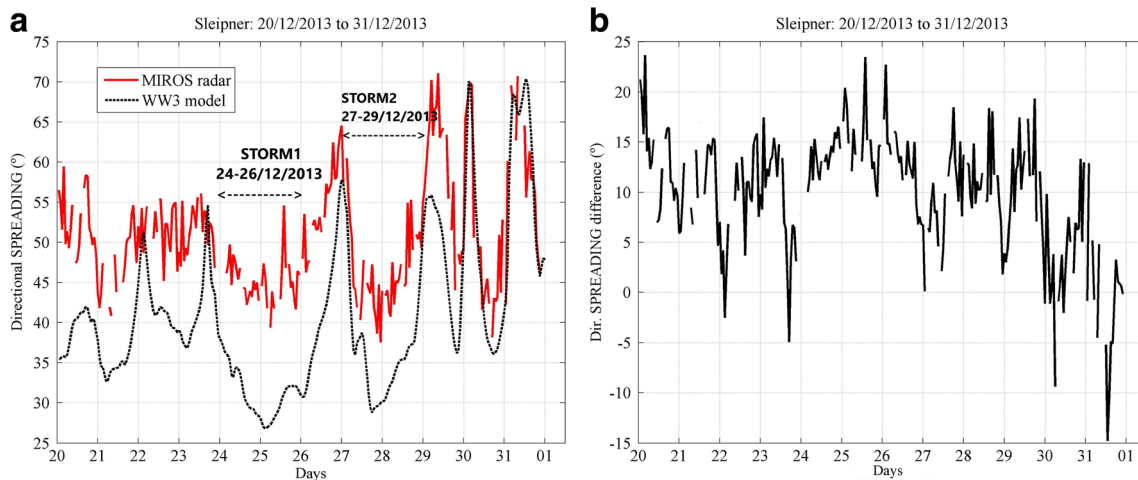


Fig. 9 Directional spreading (deg) time series from the wave model (*black dashed line*) and from the MIROS radar (*red line*). Period of 20 to 31 December 2013 (**a**). Differences between the directional spreading recorded by radar (reference) and obtained from WW3 (**b**)

showed that during the period of the study (2 months), the hindcasted directional spreading parameter was higher than the recorded values. In the present study, the directional spreading values recorded by the radar were available for a shorter period of 12 days and resulted in a wider directional spreading most of the time than the modeled values (Fig. 9).

The normalized directional distribution of spectral energy is shown in Fig. 10 for the two dates, where the differences between radar and model spectra were larger. On 25 December 2013 at 13:00 UTC, the radar shows a multimodal distribution with three peaks, whereas the model shows two peaks. On the 26 December 2013 at 01:00 UTC, both the

radar and the model show a growth in the secondary peak, but the model still shows considerable deviations from the radar distribution.

6.4 Two-dimensional wave spectra

In this section, the directional wave spectra from the radar and from the model are analyzed for the 12-day period of 20 to 31 December 2013. Spectral energy is given in the direction of propagation for model and radar spectra. In general, a good agreement between radar and model spectra was observed as can be seen in Fig. 11, where we selected the date of 27

Fig. 10 Normalized directional distribution of wave spectral energy. **a** 25 December 2013 13:00 UTC and **b** 26 December 2013 01:00 UTC. *Red line*—MIROS radar, *black dashed line*—model

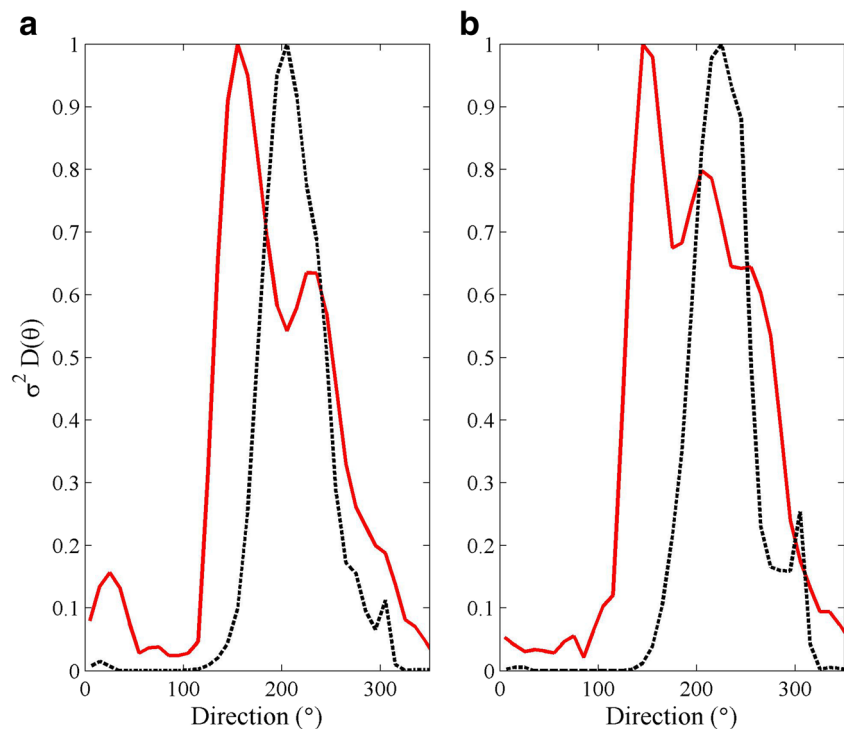
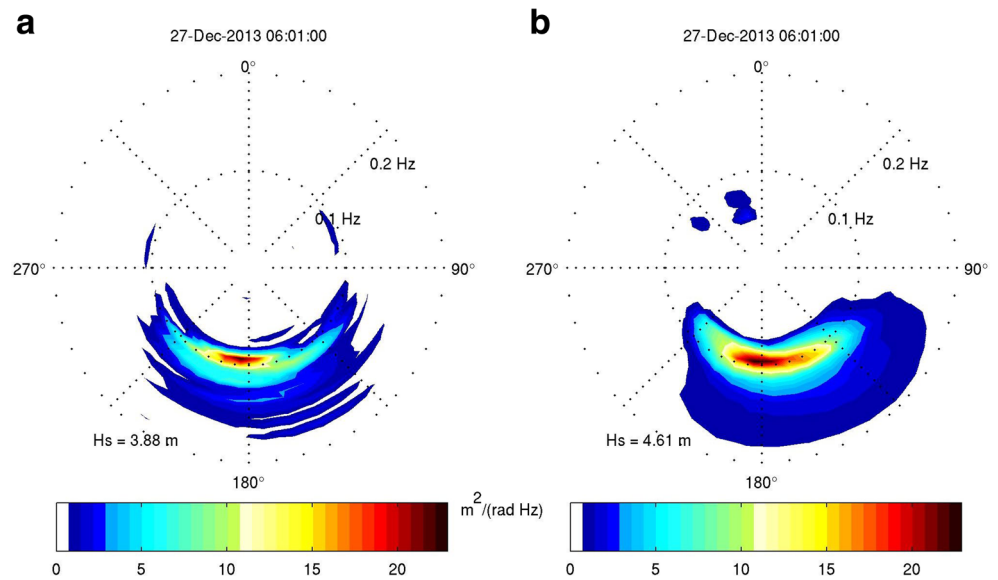


Fig. 11 Directional wave spectra on 27 December 2013 at 06:00 UTC. **a** Radar and **b** WW3



December 2013 as an example. The two-dimensional (2D) wave spectra corresponding to the two major storms were further analyzed.

On 25 December 2013 at 13:00 UTC, the difference in directional spreading between the radar and the model attains a maximum of 23.5° (Fig. 9). The directional spectrum for this date is shown in Fig. 12, where it can be observed that, while the peak frequency is similar between radar and model, the model and radar peak directions are different. The total energy is similar, judging from the H_s values, but the radar spectrum covers a sector with width of 135° between west and southeast, while the model spectrum is limited to the southwest sector.

The radar and model spectra on 26 December 2013 at 01:00 UTC are displayed in Fig. 13. The model spectrum

(Fig. 13b) has a single peak on the southwest quadrant, while the radar spectrum (Fig. 13a) shows several peaks. The most energetic is in the south-southeast sector.

The discrepancy between radar and model spectra is similar in both cases (25 December 2013 at 13:00 UTC and 26 December 2013 at 01:00 UTC) with multi-peaked radar spectra spread between northwest and southeast contrasting with single-peaked model spectra limited to the southwest quadrant.

Multi-modal sea states of the North Sea were reported by many authors as having a high frequency of occurrence (Guedes Soares 1991; Boukhanovsky et al. 2007; Ponce de León and Guedes Soares 2012). The multi-peaked spectra are the result of a combination of different factors such as the complex shape of the North Sea and complicated synoptic

Fig. 12 Directional wave spectra on 25 December 2013 at 13:00 UTC. **a** Radar and **b** WW3

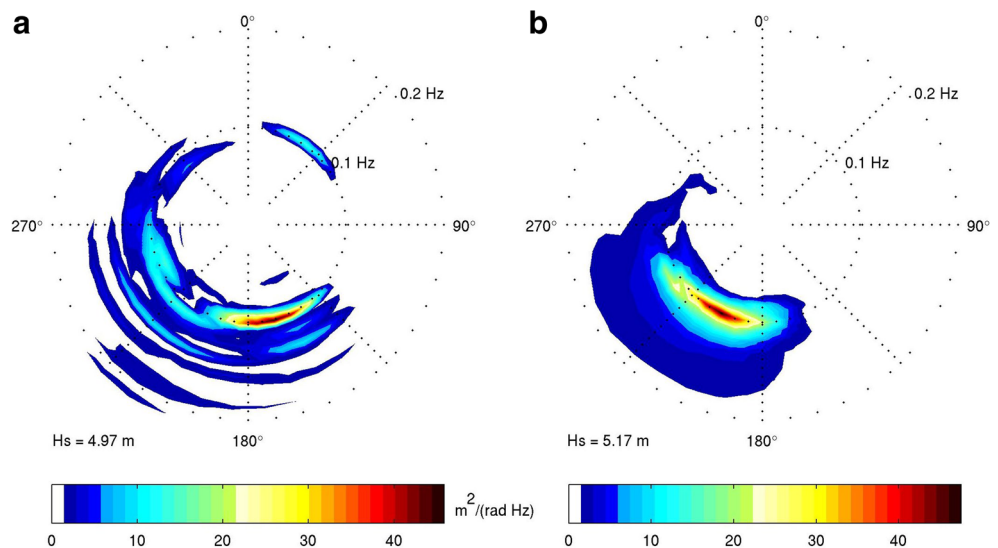
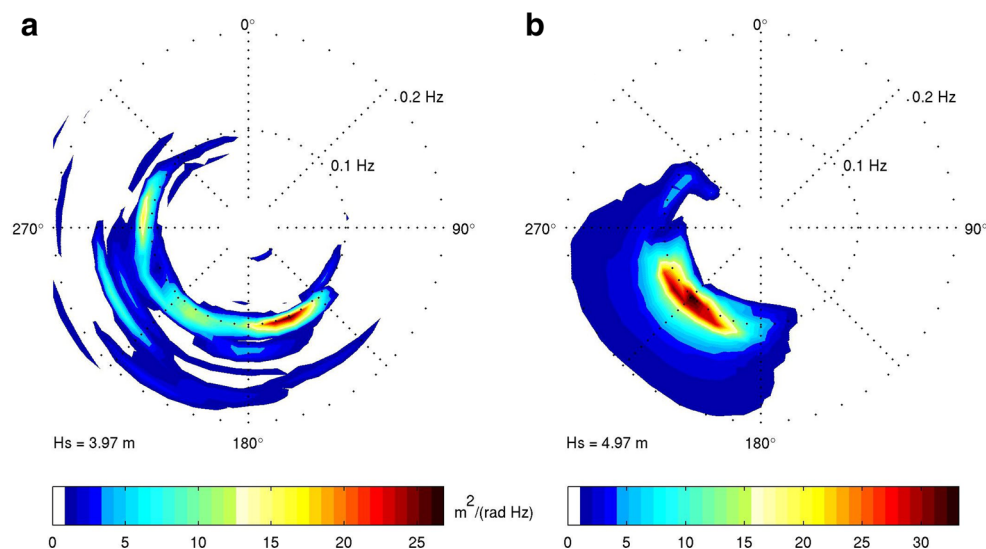


Fig. 13 Directional wave spectra on 26 December 2013 at 01:00 UTC. **a** Radar and **b** WW3



conditions as those observed in the 2013–2014 winter, where winds and waves from different directions were often recorded.

7 Conclusions

The ability of a third-generation wave model in hindcasting severe sea states was assessed for a 12-day winter period in the North Sea using buoys and microwave Doppler radar records. Integrated parameters of the sea state spectrum were accurately hindcasted by the model. The frequency spectra of the model were compared to spectra measured by the radar by means of the RMS difference, and a good agreement was found in general, although the RMS difference showed large values at the peak of two major storms. These differences were attributed to a slight shift in the peak frequency. An analysis of the source terms showed that both wind input and wave-wave nonlinear interactions were dominant. Another milder event was characterized by an underestimation of the peak spectral energy. In that case, the local process was dominated by wave-wave nonlinear interactions.

When forecasting extreme waves in a directional sea, the directional spreading of the spectrum is an important parameter. It was found that the model consistently underestimated the directional spreading when compared to the radar measurements. The most severe underestimation occurred near or at the peak of the storms. There is a need to clarify the source of these discrepancies because they occur during the most dangerous sea states, where the appearance of extreme waves is associated to severe risks to marine structures and operations.

The underperformance of the wave model at location 10 is pointing that a tuning is needed for a wide range of storm conditions of the North Sea. In addition, a reduction of the

integration time step and an increase in the number of directional bins may improve the swell propagation across the basin.

Acknowledgements The authors are very grateful to STATOIL, to Dr. Anne Karin Magnusson, and Dr. Magnar Reistad from the Norwegian Meteorological Institute who kindly supplied the MIROS radar data. The WW3 simulations were conducted on the Fionn supercomputer at the Irish Centre for High-End Computing. This work was supported by the European Research Council (ERC) under the research project ERC-2011-AdG 290562-MULTIWAVE and Science Foundation Ireland under grant number SFI/12/ERC/E2227 (<http://www.ercmultiwave.eu/>).

References

- Amrutha MM, Sanil Kumar V, Sandhya KG, Balakrishnan Nair TM, Rathod JL (2016) Wave hindcast studies using SWAN nested in WAVEWATCH III-comparison with measured nearshore buoy data off Karwar, eastern Arabian Sea. *Ocean Eng* 119:114–124
- Battjes JA, Janssen JPFM (1978) Energy loss and set-up due to breaking of random waves. In *Proc. 16th Int. Conf. Coastal Eng.*, pp. 569–587, ASCE
- Behrens A, Gunther H (2009) Operational wave prediction of extreme storms in northern Europe. *Nat Hazards* 49:387–399
- Bidlot J (2012) Intercomparison of operational wave forecasting systems against buoys: data from ECMWF, Met. Office, FNMOC, MSC, NCEP, Meteo France, DWD, BoM, SHOM, JMA, KMA, Puerto del Estado, DMI, CNR-AM, METNO, SHN-SM. August 2012–October 2012. European Centre for Medium-range Weather Forecasts. November 25, 2012
- Bidlot JR, Holmes DJ, Wittman PA, Lalbeharry R, Chen HS (2002) Intercomparison of the performance of operational ocean wave forecasting systems with buoy data. *Weather Forecast* 17:287–310
- Boukhanovsky AV, Lopatoukhin LJ, Guedes Soares C (2007) Spectral wave climate of the North Sea. *Appl Ocean Res* 29:146–154
- Cavaleri L, Burgers GJH (1992) Wind gustiness and wave growth. Memo. 00–92-18, 38 pp., Afdeling Oceanogr. Onderz., R. Neth. Meteorol. Inst., De Bilt
- Davies HC (2015) Weather chains during the 2013/2014 winter and their significance for seasonal prediction. *Nat Geosci* 8:833–837

- De Winter RC, Sterl A, Ruessink BG (2013) Wind extremes in the North Sea basin under climate change: an ensemble study of 12 CMIP5 GCMs. *J Geophys Res Atmos* 118:1601–1612
- Dobson F, Dunlap E (1999) Miros system evaluation during storm wind study II. Proc. of CLIMAR 99 WMO Workshop on Advances in Marine Climatology, Vancouver
- Eldeberky Y (1996) Nonlinear transformation of wave spectra in the nearshore zone. Ph.D thesis, Delft University of Technology, Delft
- Fedele F, Brennan J, Ponce de León S, Dudley J, Dias F (2016) Real world ocean rogue waves explained without the modulational instability. *Sci Rep* 6:27715
- Gallagher S, Tiron R, Whelan E, Gleeson E, Dias F, McGrath R (2016) The nearshore wind and wave energy potential of Ireland: a high resolution assessment of availability and accessibility. *Renew Energy* 88:1–23
- Guedes Soares C (1991) On the occurrence of double peaked wave spectra. *Ocean Eng* 18:167–171
- Hasselmann SK, Hasselmann JH, Allender TP, Barnett (1985) Computations and parameterizations of the nonlinear energy transfer in a gravity-wave spectrum, part II: parameterizations of the nonlinear energy transfer for application in wave models. *J Phys Oceanogr* 15:1378–1391
- Haver S (2000) Evidences of the existence of freak waves. In: *Rogues Waves 2000*, Brest
- Haver S, Andersen OJ (2000) Freak waves: rare realizations of a typical population or typical realizations of a rare population? Proceedings of the 10th International Offshore and Polar Engineering Conference (ISOPE), Seattle
- Janssen PAEM (1989) Wind-induced stress and the drag of air-flow over sea waves. *J Phys Oceanogr* 19:745–754
- Janssen PAEM (1991) Quasi-linear theory of wind wave generation applied to wave forecasting. *J Phys Oceanogr* 21:1631–1642
- Kettle AJ (2015) Storm Britta in 2006: offshore damage and large waves in the North Sea. *Nat Hazards Earth Syst Sci Discuss* 3(9):5493–5510
- Komen GJ, Hasselmann S, Hasselmann K (1984) On the existence of a fully developed wind-sea spectrum. *J Phys Oceanogr* 14:1271–1285
- Komen GJ, Cavaleri L, Donelan M, Hasselmann K, Hasselmann S, Janssen PAEM (1994) *Dynamics and modelling of ocean waves*. Cambridge University Press, Cambridge
- Magnusson A, Donelan M (2013) The Andrea wave characteristics of a measured North Sea rogue wave. *J OMAE* 135:031108–031101
- Mardia KV, Jupp PE (2000) *Directional statistics*. Wiley, Chichester MR1828667
- Masselink G, Castelle B, Scott T, Dodet G, Suanes S, Jackson D, Flocc F (2016) Extreme wave activity during 2013/2014 winter and morphological impacts along the Atlantic coast of Europe. *Geophys Res Lett*. doi:10.1002/2015GL067492
- Met Office Report (2014) The recent storms and floods in UK. Centre for Ecology and Hydrology, Natural Environment Research Council
- Ponce de León S, Guedes Soares C (2012) Distribution of winter wave spectral peaks in the seas around Norway. *Ocean Eng* 50:63–67
- Ponce de León S, Guedes Soares C (2015) Hindcast of the Hercules winter storm in the North Atlantic. *Nat Hazards* 78(3):1883–1897
- Ponce de León S, Ocampo-Torres FJ (1998) Sensitivity of a wave model to wind variability. *J Geophys Res* 103(C2):3179–3201
- Ponce de León S, Orfila A, Simarro G (2016) Wave energy in the Balearic Sea. Evolution from a 29 years spectral wave hindcast. *Renew Energy* 82:1192–1200
- Reistad M, Breivik Ø, Haakenstad H, Aarnes OJ, Furevik BR, Bidlot JR (2011) A high-resolution hindcast of wind and waves for the North Sea, the Norwegian Sea, and the Barents Sea. *J Geophys Res* 116(C05019):2156–2202
- Reistad M, Haakenstad H, Furevik BR, Haugen JE, Breivik O, Aarnes OJ (2015) Validation of the Norwegian wind and wave hindcast-NORA 10, MET report no. 28/2015, ISSN 2387–4201, Norwegian Meteorological Institute
- Ribeiro EO, Ruchiga TS, Lima, JAM (2013) A Brazilian northeast coast wave data comparison—radar vs buoy. ASME Proceedings of 32nd International Conference on Ocean, Offshore and Arctic Engineering OMAE2013. June 9–14, 2013, Nantes, France
- Roland A, Ardhuin F (2014) On the developments of spectral wave models: numerics and parameterizations for the coastal ocean. *Ocean Dyn* 64(6):833–846
- Tamura H, Waseda T, Miyawasa Y (2010) Impact of nonlinear energy transfer on the wave field in Pacific hindcast experiments. *J Geophys Res* 115(C12036):1–20
- Tolman HL (2002) Alleviating the garden sprinkler effect in wind wave models. *Ocean Mod* 4:269–289
- Tolman HL (2014) The WAVEWATCH III Development Group, User manual and system documentation version 4.18 Tech Note 316, NOAA/NWS/NCEP/MMAB, 282 pp
- Van Vledder G, Gautier C (2015) SWAN low-frequency wave forecasts at the North Sea an investigation to possibilities for improvement, 1220071–014, 108 pp, DELTARES